2005

Extreme impact and cavitation forces of a biological hammer: strike forces of the peacock mantis shrimp Odontodactylus scyllarus

Sheila Patek, *University of Massachusetts - Amherst*
R. L Caldwell

The Journal of Experimental Biology 208, 3655-3664
Published by The Company of Biologists 2005
doi:10.1242/jeb.01831

Extreme impact and cavitation forces of a biological hammer: strike forces of the peacock mantis shrimp *Odontodactylus scyllarus*

S. N. Patek* and R. L. Caldwell

Department of Integrative Biology, University of California, Berkeley, CA 94720-3140, USA

*Author for correspondence (e-mail: patek@berkeley.edu)

Accepted 11 August 2005

Summary

Mantis shrimp are renowned for their unusual method of breaking shells with brief, powerful strikes of their raptorial appendages. Due to the extreme speeds of these strikes underwater, cavitation occurs between their appendages and hard-shelled prey. Here we examine the magnitude and relative contribution of the impact and cavitation forces generated by the peacock mantis shrimp *Odontodactylus scyllarus*. We present the surprising finding that each strike generates two brief, high-amplitude force peaks, typically 390–480 μs apart. Based on high-speed imaging, force measurements and acoustic analyses, it is evident that the first force peak is caused by the limb's impact and the second force peak is due to the collapse of cavitation bubbles. Peak limb impact forces range from 400 to 1501 N and peak cavitation forces reach 504 N. Despite their small size, *O. scyllarus* can generate impact forces thousands of times their body weight. Furthermore, on average, cavitation peak forces are 50% of the limb's impact force, although cavitation forces may exceed the limb impact forces by up to 280%. The rapid succession of high peak forces used by mantis shrimp suggests that mantis shrimp use a potent combination of cavitation forces and extraordinarily high impact forces to fracture shells. The stomatopod's hammer is fundamentally different from typical shell-crushing mechanisms such as fish jaws and lobster claws, and may have played an important and as yet unexamined role in the evolution of shell form.

Supplementary material available online at
http://jeb.biologists.org/cgi/content/full/208/19/3655/DC1

Key words: stomatopoda, crustacea, fracture, biomechanics, force, impact, cavitation, mollusca, shell, evolution, peacock mantis shrimp, *Odontodactylus scyllarus*.

Introduction

Shell-breaking is widespread in the animal kingdom. Most species crush shells by cyclically applying loads with low peak forces and large impulses (forces applied over long time periods), including mechanisms such as fish and reptile jaws, decapod claws and cephalopod beaks (Grubich, 2000; Herrel et al., 2002; Moody and Steneck, 1993; Vermeij, 1987; Voight, 2000). In contrast to these crushing mechanisms, hammers generate pounding blows with high peak forces delivered over short time periods. Mantis shrimp are the most speciose and geographically widespread group of organisms to use an appendage as a hammer; there are only a few other biological examples (Vermeij, 1987), which include snapping shrimp (Beal, 1983), several bird species (Butler and Kirbyson, 1979; Snyder and Snyder, 1969), Ankylosauria tails (Coombs Jr, 1979) and human karate practitioners (Walker, 1975; Wilk et al., 1983).

Mantis shrimp (Crustacea, Stomatopoda) use their greatly enlarged second thoracic raptorial appendages to smash or spear prey, construct and excavate burrows, defend against predators and fight with conspecifics (Caldwell, 1975). In 'spearer' stomatopods, the dactyl is a sharp, spiny, barbed spear, which stabs into soft-bodied, evasive prey. 'Smasher' stomatopods can stab with the sharp tip of their dactyl or smash with the bulbous heel of the dactyl (Fig. 1). In order to generate extreme accelerations with their raptorial appendages, all mantis shrimp species are thought to utilize a power amplification mechanism consisting of elastic springs, latches and lever arms (Burrows, 1969; Burrows and Hoyle, 1972; McNeill et al., 1972; Patek et al., 2004). The click mechanism holds the limb in place during muscle contraction (Burrows, 1969; Burrows and Hoyle, 1972; McNeill et al., 1972), and a specialized spring stores and releases elastic energy (Patek et al., 2004). The subject of the present study, the 'smasher' peacock mantis shrimp *Odontodactylus scyllarus*, can deliver strikes lasting only a few milliseconds, with accelerations of over 10^5 m s^{-2} and speeds of over 20 m s^{-1} (Fig. 1; Patek et al., 2004).

One unexpected consequence of these extreme strike speeds is the generation of cavitation at the site of impact between the mantis shrimp's heel and the striking surface (Fig. 1; Patek et al., 2004). Cavitation vapor bubbles form in fluids under low pressure. This may be caused by adjacent flow fields moving

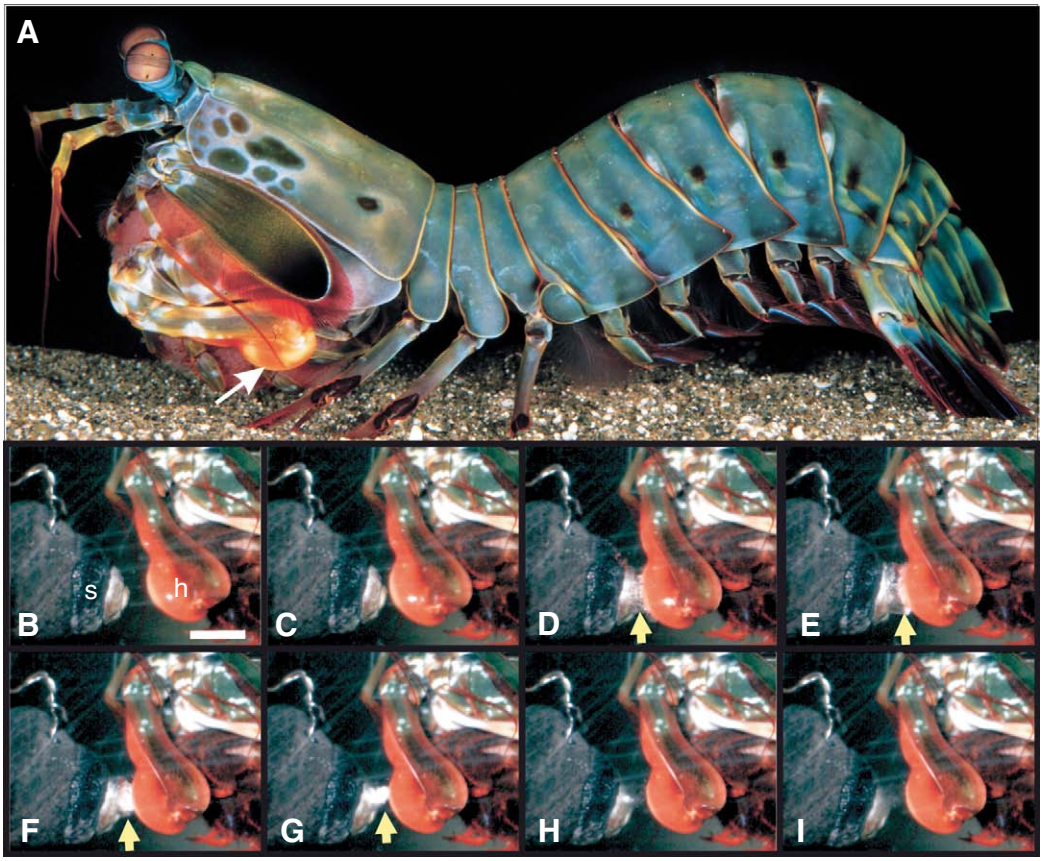

Fig. 1. Peacock mantis shrimp use a pair of large raptorial appendages (A, white arrow) to strike hard objects with such high speeds that cavitation bubbles form between the appendage and striking surface (Patek et al., 2004). (B–I) The dactyl heel (h) of the raptorial appendage strikes a snail (s) that is loosely wired to a stick. Images recorded at 0.2 ms intervals. Scale bar, 1 cm. Cavitation (yellow arrow) is visible between the dactyl heel and snail (D–G).

at drastically different speeds and, at their interface, generating regions of low pressure (Brennen, 1995; Young, 1999). Thus, cavitation often occurs between a solid structure's boundary layer and a rapid flow field over its surface. Vortex cavitation commonly occurs in the vortices shed by pumps and boat propellers, while sheet cavitation often develops in a wake or area of separated flow and is visible along propeller blades and hydrofoils. Cavitation generated during the mantis shrimp's strike (Patek et al., 2004) is most likely caused by a combination of these flow processes, including sheet cavitation along the surfaces of the snail shell and dactyl, and the negative pressure generated during the rapid rebound of the dactyl heel after striking the hard surface (Fig. 1).

When cavitation bubbles collapse, considerable energy is released in the form of heat, luminescence and sound (Brennen, 1995). The shock waves and microjets generated during the collapse of the cavitation bubbles cause stress and fatigue in adjacent surfaces, ultimately leading to failure and flaking of surface materials (Brennen, 1995). Remarkably, a 2.7 mm cavitation bubble collapsing near a wall can generate over 9 MPa of impact pressure over a period of approximately 5 μs (Shima et al., 1983; Tomita et al., 1983). Such cavitation forces can destroy rapidly rotating boat propellers, aid in water-based metal cutters, and are even thought to provide the mechanism by which water picks remove dental plaque (Brennen, 1995).

Cavitation has been documented in several biological systems. Most biological examples of cavitation are caused by low pressure fluid tension in enclosed spaces, such as tree xylem (Smith, 1994; Tyree et al., 1984; Tyree and Sperry, 1989), octopus suckers (Smith, 1991; Smith, 1996), human metacarpophalangeal joints (Unsworth et al., 1971), fern sporangia (Ritman and Milburn, 1990) and fungal spores (Milburn, 1970; Money et al., 1998). By contrast, perhaps the most dynamic example of biological cavitation is found in snapping shrimp, which shoot cavitation bubbles to stun their prey (Lohse et al., 2001; Versluis et al., 2000). The snapping claw closes and shoots a water jet at extreme speeds, which causes negative pressure and associated cavitation behind the water jet (Lohse et al., 2001; Versluis et al., 2000). Indeed, the loud popping noises heard in many oceans are generated by the collapse of cavitation bubbles during snapping shrimp strikes (Versluis et al., 2000).

The presence of cavitation is often detected acoustically because the sound of cavitation bubbles collapsing contains greater energy at higher frequencies than similar events without cavitation (Brennen, 1995; Lush and Angell, 1984; Martin et al., 1981). Thus, the acoustic signature of cavitation is the presence of a broadband signal extending, with substantial energy, into the ultrasonic range (above 20 kHz), as compared to events without cavitation that lack power in the ultrasonic acoustic range. This phenomenon has been examined extensively in the engineering literature, including controlled studies in which cavitation is present and absent, as well as correlative studies linking cavitation damage with the

acoustic power of the signal in the ultrasonic range (Brennen, 1995; Ceccio and Brennen, 1991; Lush and Angell, 1984; Martin et al., 1981). Cavitation has also been detected *via* acoustic analyses, especially in the ultrasonic range, in studies of tree xylem cavitation (Ikeda and Ohtsu, 1992; Perks et al., 2004; Tyree et al., 1984) and fern sporangia (Ritman and Milburn, 1990).

The presence and dynamics of cavitation can also be detected visually. Extreme high-speed video is necessary to capture the microsecond timescales of cavitation bubble formation, luminescence and collapse. Cavitation bubbles in snapping shrimp were visualized using high-speed video, coupled with the use of a photodector to detect the emission of luminescence (Lohse et al., 2001). The simple presence/absence of cavitation vapor bubbles has been examined in x-rays of joints after knuckle-cracking in humans (Unsworth et al., 1971) and light microscope images of fungal spores (Money et al., 1998).

Despite our rich understanding of crushing forces and their influences on shell evolution, as well as a substantial body of work on the physics of cavitation, little is known about the impact forces generated by biological hammers and biological cavitation. The mantis shrimp's unusual mechanism for breaking shells suggests fundamental questions about the amplitude of the limb impact forces and relative contribution of cavitation forces. Here, through the use of force transducers, acoustic analyses and high-speed video, we report the limb impact and cavitation forces generated by the peacock mantis shrimp *Odontodactylus scyllarus*. The goals of this study were to (1) visualize limb impact and cavitation while measuring forces, specifically to identify the presence and relative contribution of cavitation to force generation; (2) measure the timing and acoustic signature of impact and cavitation; and (3) measure amplitude of forces across a range of striking surface geometries in order to assess the effects of striking surface on the amplitude of cavitation and impact forces. This study provides the first in-depth examination of a biological hammer and reveals a potent combination of power amplification, extreme impact forces and cavitation dynamics.

Materials and methods

Study animals

Thirteen peacock mantis shrimp *Odontodactylus scyllarus* L. (Crustacea, Stomatopoda, Gonodactyloidea, Odontodactylidae), ranging in size from 27 to 36 mm carapace length, were purchased from commercial collectors. Animals were held at 25°C in recirculating artificial saltwater, and were fed a diet of fresh snails and freeze-dried and frozen shrimp. Because of their unpredictable molt cycles, different combinations of individuals were used in each of the experiments. During a molt, animals were unable to strike for several days, and only gradually recovered full striking strength. We therefore tested animals only when they were in an intermolt period. Animals regularly struck objects coated with shrimp paste and most animals were willing to strike objects under bright video lights after a period of training. In natural conditions, peacock mantis shrimp carefully position a snail on a firm surface or anvil-like rock, and then deliver a blow that typically causes little movement of the snail. In this study, a force sensor (load cell) was mounted at the base of an aluminum beam that was manually presented to the mantis shrimp. This arrangement permitted minimal movement of the apparatus when struck.

Synchronous high-speed video and force sensor analysis of force peaks

Cavitation processes were visualized through the use of high-speed video. Digital video images were collected at 100 000 frames s^{-1} (~0.3 mm $pixel^{-1}$, 10 μs shutter speed, Ultima APX high speed camera and Multi Channel Data Link, Photron, San Diego, CA, USA) and were synchronized with a one-axis force sensor (force range 444.8 N, upper frequency limit 75 kHz, Model 200B02, PCB Piezotronics, Depew, NY, USA) sampled at 100,000 samples s^{-1}. The kinematics of the recorded movements were analyzed using a custom computer program (Matlab v7.0.1, The Mathworks, Natick, MA, USA). The distance moved by the limb across each frame was calibrated, using a structure within the image sequence with known dimensions.

Acoustic analyses of impact and cavitation

In addition to image analysis, we measured the acoustic signatures of limb impact and cavitation. We simultaneously measured strike forces and sound when mantis shrimp struck curved and flat force-sensor surfaces. Sounds generated during strikes on curved and flat surfaces were measured using a hydrophone (1–170 kHz TC4013 hydrophone, 1 Hz–1 MHz VP2000 voltage preamplifier; Reson Inc., Goleta, CA, USA). Acoustic data were collected at 500 000 samples s^{-1}, using a data acquisition board (PCI-DAS4020/12, Measurement Computing, Middleboro, MA, USA) and custom computer data acquisition programs (Matlab v7.0.1). The onset of the first peak was detected automatically with a threshold of 0.05 V above the average value of a 100-sample window. The second peak onset was set at 0.05 V above the average value of a 40-sample window following the first peak. The second peak duration was set to the same duration as the first peak.

The power spectral density of each acoustic peak was calculated using a multitaper method (discrete-time Fourier transform, nonparametric pmtm periodogram, Matlab v7.0.1). The short duration of the Fourier transforms resulted in a loss of low frequency resolution below approximately 2 kHz. The maximum amplitude of the acoustic data was scaled to 1 V prior to comparing the power spectral density across events. For the flat surface tests, acoustic data were collected for five individuals (3–5 strikes per individual). For the curved surface tests, acoustic data were collected from six individuals (4–21 strikes per individual).

One-axis analysis of impact and cavitation forces

We used a one-axis force sensor to measure the relative

contributions of limb impact force and cavitation force (force range 444.8 N, upper frequency limit 75 kHz, Model 200B02, PCB Piezotronics, NY, USA). The stainless steel force sensor had a 12.7 mm diameter load surface and a stiffness of 1.9 kN μm^{-1}. Data were collected at 500,000 samples s^{-1} using a data acquisition board (NIDAQ 6062E, National Instruments, Austin, TX, USA). Peak forces (amplitude of force trace) and force impulse (integrated area under a force curve; Caldwell et al., 2004; Ozkaya and Nordin, 1999) were analyzed using custom-designed computer analysis tools (Matlab v7.0.1). The onset of the first peak was set as an increase of 0.05 V above the average value of a 100-sample window. The second peak onset was set at 0.08 V above a 40-sample average window after the first peak. The ends of the first and second peaks were set to the same value as the onset voltage for each peak.

Video recordings (60 frames s^{-1}, Sony DCR-VX2100, Sony Corp., New York, NY, USA) were simultaneously collected in order to establish whether the force sensor was struck by one or both raptorial appendages. Both peaks were analyzed if only one raptorial appendage struck the force sensor. If two raptorial appendages struck the force sensor in close succession, four force peaks were logged, leading to potential ambiguity as to the source of each of the four peaks. In these cases, only the first peak was included in the analysis. Some individuals exceeded the capacity of the load cell, thus any force data that exceeded the linear range of the load cell (>445 N) were removed. After the overloaded data had been removed, the final dataset reported here included four individuals with 6, 12, 22 and 25 strikes per individual.

Three-axis force analyses of strikes on curved and flat surfaces

We measured the effects of surface geometry on force generation through the use of curved and flat surfaces. For the curved sensor, we measured the radius of curvature of a range of snails typically consumed by these mantis shrimp and machined a curved cap for the force sensor with the average measured radius of curvature (9.7 mm curvature; 28.5 mm solid, 300-series stainless steel from strike surface to sensor surface). The flat sensor was 24.1 mm×24.1 mm, with 18.1 mm solid, 300-series stainless steel from strike surface to sensor surface.

Strike forces on curved and flat surfaces were compared using a waterproof, three-axis, piezoelectronic force sensor designed for measuring impact forces (force range 1334 N in each axis, 90 kHz upper frequency limit, <4.1% cross-talk between axes; W20M25/010G10, PCB Piezotronics). The *z*-axis was designated as a horizontal force 'into' the sensor. The *y*-axis was defined as a vertical force, and the *x*-axis represented lateral forces.

The stainless steel sensor provided a reasonable, although not perfect, approximation of mollusk shell material properties. For comparison, mollusk shells have tensile strength ranging from 30–167 MPa, Young's modulus of elasticity (stiffness) 30–70 GPa, and Vicker's hardness ranging from 110 to 250 kg mm^{-2} (Vincent, 1990). 300-series stainless steel typically has a tensile strength (to yield) of 200–300 MPa, modulus of elasticity of 193 GPa, and Vicker's hardness of 139–169 kg mm^{-2} (product data sheets; Harvey, 1985).

The peak amplitude of forces in the three axes was measured using a custom, automated computer program and forces from each axis were summed using standard vector calculations (Matlab v7.0.1). The onset threshold of the first force peak was set as 0.02 V above the average value of a 100-sample window; the onset of the second force peak was set as 0.05 V over a 40-sample average window following the first peak.

The thick and heavy steel caps on the three-axis force sensor generated long reverberations, which prevented unambiguous quantitative measurements of impulse at less than 1 ms after the initial impact. Thus, although we could measure the amplitude and the relative timing of the multiple peaks, it was not possible to report conclusive impulse data after the initial force peak. Some animals exceeded the capacity of this force sensor and these data were removed from the analyses. With these data removed, our final dataset included, for the flat sensor tests, ten individuals (5–20 strikes per individual) and for the curved sensor tests, six individuals (4–23 strikes per individual). Video recordings (60 frames s^{-1}; Sony DCR-VX2100, Sony Corp.) were simultaneously collected in order to establish whether the force sensor was struck by one or both raptorial appendages.

Statistical analyses

Values are means ± S.D. One-way analysis of variance (ANOVA) was used to assess individual variation in the temporal aspects of force generation. The scaling of force with carapace length and dactyl heel width was evaluated with a linear regression. Statistical software was used for these calculations (JMP 5.0.1, SAS Institute, Inc., Cary, NC, USA).

Results

Synchronous high-speed video and force sensor analysis of force peaks

Cavitation vapor bubble formation, collapse and rebound were visible with ultra-high speed imaging. We analyzed the temporal correlation between force generation, limb impact and cavitation bubble collapse using the video and force data. A single strike by a single appendage generated two force peaks in rapid succession (Figs 2, 3). The individual mantis shrimp used in this study only had one raptorial appendage, thus allowing us to rule out fast double-strikes as the cause of the two force peaks. In all strike sequences, the first force peak corresponded with limb impact and the second force peak occurred during cavitation bubble collapse (Figs 2, 3). Videos are available online as supplementary material.

Acoustic analyses of impact and cavitation

Consistent with the video analysis above, each strike generated two peaks in both the force data and acoustic data, regardless of whether the striking surface was curved or flat

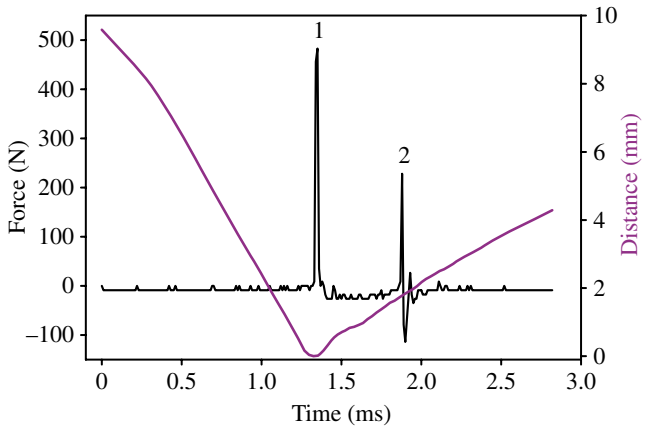

Fig. 2. Limb movement and force generation. The heel of the raptorial appendage (purple, right *y* axis) approaches the force sensor (located at distance 0, right *y* axis) and generates force (black, left *y* axis) during impact (peak 1) and when cavitation bubbles collapse (peak 2). Negative pressure as the limb rebounds from the sensor surface is indicated by the slight negative excursion of the force trace between the first and second force peaks. Distance data was digitized from high-speed video (100,000 frames s^{-1}) and smoothed using the negative exponential function (polynomial regression and Gaussian density function; SigmaPlot v.9.0, Systat). The one-axis force sensor was sampled simultaneously at 100,000 samples s^{-1}.

(Fig. 4). Spectral power analysis showed that second acoustic peaks typically contained more energy at higher frequencies (above 40 kHz) than first peaks in both curved and flat surface experiments (Fig. 5, Table 1). The times between the first and second acoustic peaks were 390±54 μs on the curved surface and 472±49 μs on the flat surface (Table 2).

One axis analysis of impact and cavitation forces

We used a one-axis force sensor to measure the relative contribution of limb impact force and cavitation force, both in terms of peak force and impulse (Fig. 6). We found that the cavitation forces were an average of 50% of the limb impact forces, and reached a maximum of 280% of the limb impact force within a given strike (Table 3). The ratio of the second

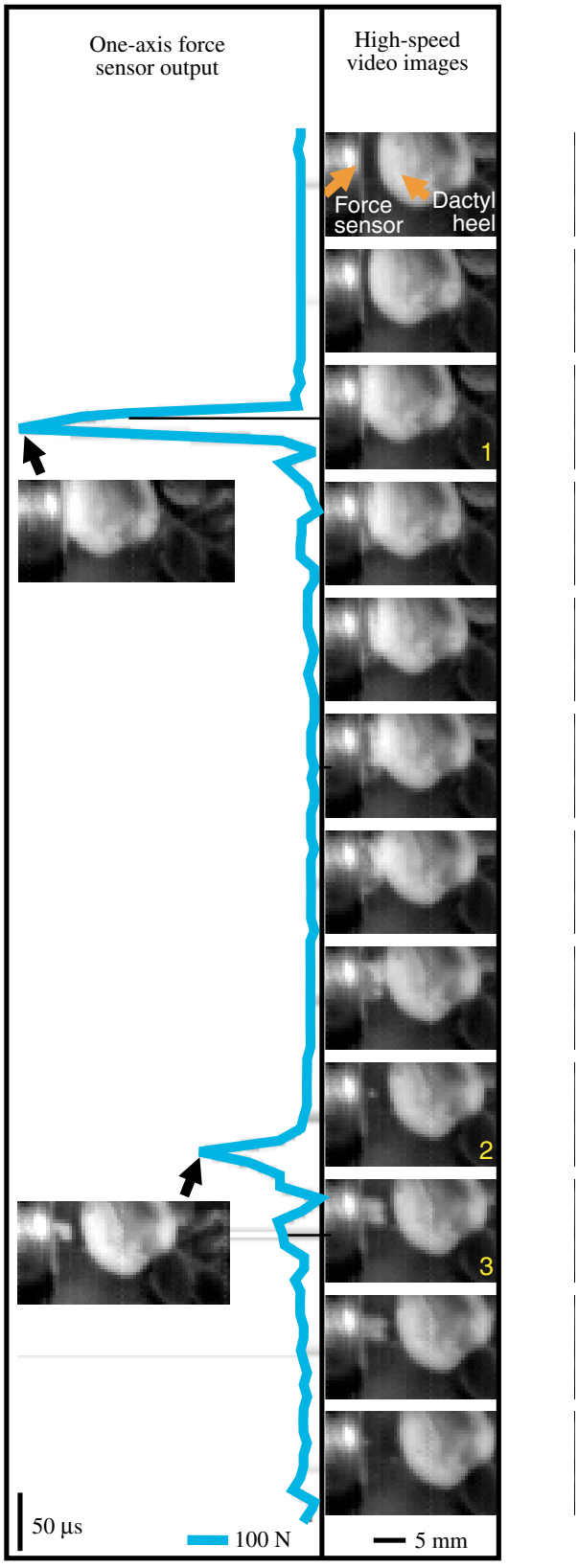

Fig. 3. The formation, collapse and rebound of a cavitation bubble between a mantis shrimp's dactyl heel and a force sensor. The left trace (blue) indicates force output from a force sensor that was recorded synchronously with high-speed images at 100,000 samples s^{-1}. The series of photographs on the right are recorded at 0.1 ms intervals (from the top down) and temporally aligned with the horizontal lines in the force trace. The two images on the left correspond with the two maximal force peaks. The formation of a cavitation bubble begins when the limb strikes the force sensor (1). The cavitation bubble collapses at the onset of the second peak (2), and then rebounds (3) until the last shown image. This sequence of cavitation bubble formation, collapse and rebound is typical of cavitation occurring near a boundary, in which peak force occurs during cavitation bubble collapse (Brennen, 1995; Tomita and Shima, 1990). Termed the rebound phase, a small cloud of bubbles is typically formed after the initial collapse of the primary cavitation bubble. These smaller bubbles will continue to collapse, but with smaller resultant forces than the collapse of the first large cavitation bubble (Brennen, 1995; Tomita and Shima, 1990). Videos of simultaneous force and video traces are available online as supplementary material.

peak to the first peak force was not significantly different across individuals in the peak force, but the ratio of the second impulse to the first impulse did vary significantly across individuals (one-way ANOVA; peak force: P=0.8486; impulse: P=0.0004). The average time between the first and second peak was 410±60 μs (Table 2), with significant differences across individuals (one-way ANOVA, P<0.0001). The duration of the first peak averaged 49±18 μs and the second peak averaged 66±28 μs.

Three-axis force analyses of strikes on curved and flat surfaces

The three-axis force sensor showed that cavitation forces were typically half the amplitude of the limb impact forces, although in some strikes, the cavitation forces reached 140% of the limb impact forces (Table 4). The average time between impact and cavitation was 390±54 μs for the curved surface and 480±71 μs for the flat surface (Table 2). The ratio of the second peak force to the first peak force was not consistently significantly different across individuals (one-way ANOVA; curved cap, P=0.7264; flat cap, P=0.0009). Time between the first and second force peak was significantly different across individuals (one-way ANOVA; curved cap, P <0.0001; flat cap, P=0.0015).

Limb impact generated an average 472 N peak force summed across the three axes on the curved surface and 693 N

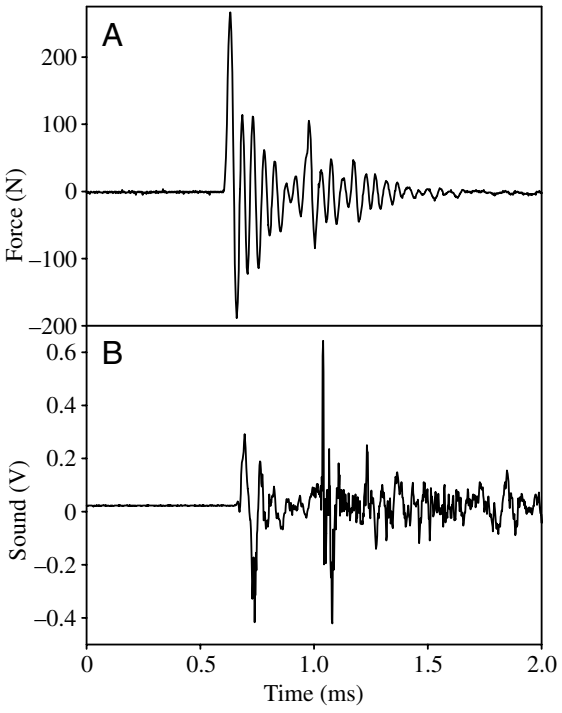

Fig. 4. Typical strike force (A) and sound (B) of a single limb striking a three-axis force sensor (only the z-axis data are shown here). Note that there is a slight offset in timing between the force and acoustic data; this offset is due to the approximately 62 μs necessary for the sound waves to reach the hydrophone, which was located several cm from the force sensor.

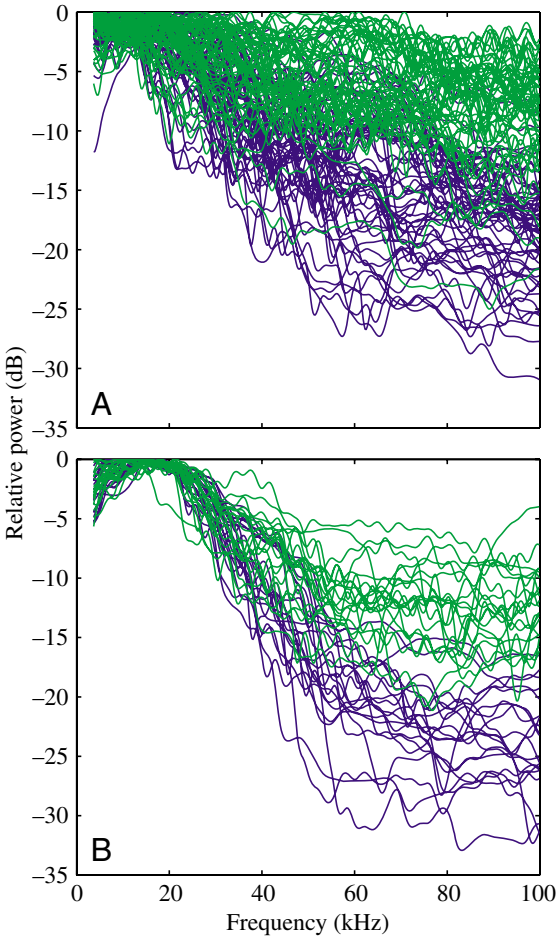

Fig. 5. Comparison of relative power spectra between the first (blue) and second (green) acoustic peaks recorded as mantis shrimp struck a three-axis force sensor. The curved surface (A) and flat surface (B) yielded similar spectral distributions. Second peaks (green) typically contained more energy at higher frequencies in the ultrasonic range (above 20 kHz) than first peaks, which is consistent with cavitation being the source of the second peak (Brennen, 1995; Lush and Angell, 1984; Martin et al., 1981). The peak amplitudes of the acoustic recordings were scaled to 1.0 prior to conducting Fast Fourier Transforms, thereby allowing comparisons of relative power/frequency of first and second peaks within a given strike and across strikes.

Table 1. *Comparison of acoustic amplitude and power outputs of first and second acoustic peaks within strikes*

	Ratio within strikes (second peak):(first peak)	
	Peak amplitude	Average power
Curved surface		
Maxima	1.2–3.2	1.7–4.6
Mean (S.D.)	1.7 (0.5)	1.6 (0.8)
Flat surface		
Maxima	2.0–2.9	1.3–2.1
Mean (S.D.)	1.8 (0.5)	1.2 (0.3)

Table 2. *Average temporal offset between first and second peaks as measured with sound, a curved force sensor and a flat force sensor*

	Time (μs)		
Data	Flat surface (1-axis)	Curved surface (3-axis)	Flat surface (3-axis)
Force	410 (60)	390 (54)	480 (71)
Acoustic	NA	390 (54)	472 (49)

Values are means ± S.D. NA, not applicable.

Table 3. *Cavitation and limb impact forces on a flat, one-axis force sensor*

	Limb impact	Cavitation	Ratio within strikes (cavitation):(impact)
Peak force (N)			
Maxima	233–420	169–386	0.91–1.43
Mean (S.D.)	226 (75)	135 (76)	0.58 (0.26)
Impulse (μNs)			
Maxima	0.17–0.77	0.07–0.63	0.46–2.80
Mean (S.D.)	0.23 (0.13)	0.13 (0.08)	0.60 (0.34)

on the flat surface, with maximum recorded forces reaching 983 N and 1501 N, respectively (Table 4). For the curved surface, animals generated peak forces of 1118–1917 times their body weight. With the flat surface, individuals generated peak forces of 1420–2624 times their body weight.

The majority of the force was delivered through the *z*-axis with similar force profiles for both flat and curved sensors (flat: *z*, 77±7%; *y*, 12±5%; *x*, 11±6%; curved: *z*, 79±7%; *y*, 12±5%; *x*, 9±7%; all values mean ± S.D.).

A narrow size range of animals was sampled for this study, but some size/force correlations were identified that were consistent across both log-transformed and raw data. Carapace length (range: 26.7–35.8 mm) was not correlated with force amplitude in the raw curved cap data; however, log-transformed data mean force was correlated with carapace length (r^2=0.8332, P=0.0305, scaling exponent=1.78). Also in the curved cap data, the width of the leading surface of the dactyl heel (range: 3.7–5.6 mm) was significantly correlated with summed force across three axes [linear regression, maximum force: r^2=0.8897, P=0.0039 (raw data) and r^2=0.8902, P=0.0047, scaling exponent=2.14 (logged data); mean force: r^2=0.8636, P=0.0073 (raw data) and r^2=0.8274, P=0.0119, scaling exponent=1.39 (logged data)]. In the flat cap surface data, carapace length was not correlated with force (P>0.6) and, again, the dactyl heel width was significantly correlated with the summed force across three axes [linear regression, maximum force: r^2=0.4827, P=0.0258 (raw data) and r^2=0.5618, P=0.0126, scaling exponent=1.95 (logged data); mean force: r^2=0.4772, P=0.0270 (raw data) and r^2=0.5615, P=0.0126, scaling exponent=1.64 (logged data)].

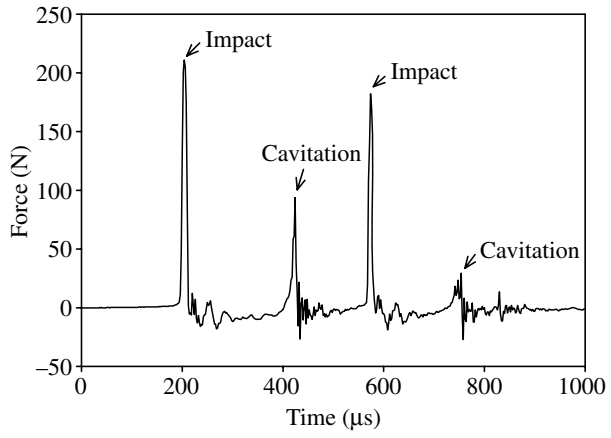

Fig. 6. Force generated when a mantis shrimp strikes with both raptorial appendages. Four force peaks are detected by a one-axis force sensor when struck by two raptorial appendages. Based on the high-speed video and acoustic analyses above, the two higher peak forces were generated by limb impact and the two lower peaks were generated during cavitation bubble collapse.

Discussion

Shell-breaking forces have historically been analyzed in terms of two predator strategies: crushing (repeated compression of whole shell until failure) and peeling (chipping away the lip of a shell until soft tissue is exposed). A single pulse of compressive crushing force, sufficient to break sturdy molluscan shells, ranges from hundreds to thousands of Newtons applied over a period of seconds (Vermeij, 1987; Vermeij and Currey, 1980). On the other hand, effective peeling requires a fraction of these crushing forces (Preston et al., 1996). Studies of the maximum force generated by crushing and peeling mechanisms suggest that predators are constrained to breaking shells below a certain size, or that predators repeatedly apply forces that gradually cause cumulative fractures in the shells (Preston et al., 1996). Indeed, predators most typically apply crushing forces multiple times for each shell, with each force application lasting for periods of hundreds of milliseconds up to multiple seconds (e.g. Kaiser

Table 4. *Peak forces generated by cavitation and limb impact on curved and flat 3-axis force sensors*

	Limb impact (N)	Cavitation (N)	Ratio within strikes (cavitation):(impact)
Curved surface			
Maxima	398–983	187–390	0.46–1.00
Mean (S.D.)	472 (125)	179 (55)	0.40 (0.10)
Flat surface			
Maxima	499–1501	256–504	0.57–1.40
Mean (S.D.)	693 (174)	348 (116)	0.54 (0.14)

Limb impact is reported as the vector sum of the three axes.

Cavitation forces in the *x* and *y* axes were negligible, so these forces are reported from the *z* axis only.

The cavitation:impact ratio is calculated from the *z* axis only.

et al., 1990; Korff and Wainwright, 2004; Zipser and Vermeij, 1978).

In contrast to crushing and peeling mechanisms, the mantis shrimp's hammer generates forces ranging from hundreds to over a thousand Newtons, delivered over microsecond timescales (Tables 3, 4). A strike with a single appendage generates two force peaks, approximately 0.5 ms apart, with the first force peak caused by limb impact and the second peak generated by cavitation bubble collapse (Figs 2–4). A strike with both appendages, therefore, generates four force peaks in extremely rapid succession (Fig. 6), at time scales on the order of 1000 times shorter than typical, cyclically applied, crushing forces.

While the absolute values of these peak forces are well within the range of crushing forces, mantis shrimp generate forces that are thousands of times their body weight, exceeding, by far, previous estimates of maximum force production (on the order of hundreds of times body weight) (Alexander, 1985; Taylor, 2000). Thus, the hammering mechanism allows mantis shrimp to generate peak forces that far surpass the peak forces generated by shell-crushers of similar body size. However, these high force peaks are delivered over very short time periods, typically 49 μs and 66 μs, for the impact and cavitation forces, respectively. As a result, the impulses of the strikes are typically on the order of a fraction of a μNs.

Inelastic impacts on hard substrates cause a rapid change in acceleration over a very short time period and thereby generate high peak forces and low impulses. The material properties of a substrate can influence the recorded peak forces, through the time course of this change in acceleration and associated absorption of energy. Thus, the peak forces produced by mantis shrimp in this study should be interpreted in the context of the steel surfaces that they struck; a more energetically absorptive surface would yield lower peak amplitudes. However, the presence of cavitation appeared not to be influenced by the material properties of the striking surface; cavitation was consistently observed in naturalistic strikes of force sensors and snail shells (e.g. Figs 1, 3) and even when animals struck rubber corks (R.L.C. and S.N.P., personal observation). It is worth noting that the particular strategy employed by mantis shrimp, that of using sequential applications of brief high magnitude forces, is well known to engineers as an effective mechanism for fracturing composite materials, specifically *via* rapid jets and ballistic impacts (Meyers, 1994).

Perhaps even more surprising than the high peak forces is the observation that mantis shrimp couple these impact forces with the implosive force of cavitation bubble collapse. While on average the cavitation forces were half those of the impact forces, in many cases the cavitation force actually exceeded those of the limb's impact (Tables 3, 4). In both the thin-surface, one-axis force sensor and the thick, solid steel, three-axis force sensors, cavitation forces played a substantial role in force generation, suggesting that this phenomenon is robust across surface geometries, surface thickness and mass (Tables 2–4). The combination of impact fractures and the surface stresses caused by cavitation may be effective for damaging the composite, ceramic layers of a mollusk shell (Vincent, 1990). In future studies, it would be informative to mount strain gauge force transducers to actual shells and to examine the relative damage imposed by limb impact and cavitation forces, especially in relation to the material properties of a shell. Indeed, to our knowledge, experimental tests of shell fracture mechanics in response to hammering with an appendage have not been previously studied.

Acoustic analyses of mantis shrimp strikes also yielded information about the presence of cavitation. The majority of the acoustic power was contained in the collapse of the cavitation bubble, with the acoustic power of the cavitation bubble collapse averaging 1.2–1.6 times the acoustic power of the limb impact (Table 1). The spectral distribution of the two sound peaks differed primarily in the ultrasonic range (Fig. 5), thereby supporting the hypothesis that the second acoustic peak was generated by cavitation bubble collapse, which is characterized by a broadband acoustic signature with substantial energy into the ultrasonic range (Brennen, 1995; Lush and Angell, 1984; Martin et al., 1981). Ultrasonic acoustic measurements of mantis shrimp strikes may be helpful in future studies for establishing the presence and absence of cavitation under different depth conditions or when smashing particular substrates, specifically through identification of two acoustic peaks and the presence of a broadband ultrasonic signature in the second peak.

The role of cavitation and control of cavitation by biological systems remains an interesting and wide-open area of biological research, and perhaps it is time to consider the evolutionary history of cavitation, even if only as an epiphenomenon. Cavitation phenomena are sensitive to ambient pressure and impurities in the water, such that cavitation bubbles form more readily at low pressures and in aerated and impure water (such as saltwater). Thus, it would be interesting to incorporate depth as a factor in evolutionary analyses of biological cavitation structures, because organisms at depths of greater than 100 m are far less likely to induce cavitation (Smith, 1996).

The subject of this study, *O. scyllarus*, is a shallow water species and is typically found to a depth of 3–30 m (Ahyong, 2001; Manning, 1967). However, the genus *Odontodactylus* includes some of the deepest living smasher stomatopods. While most odontodactylids are found living shallower than 50 m, *O. hawaiiensis* occurs to depths of greater than 100 m (Manning, 1967; Retamal, 2002) and *O. brevirostris* has been reported to depths of over 400 m, although generally this species is found in the 15–40 m range (Manning, 1967). Most other Gonodactyloidea smashers are found at less than 40 m, although several occur to 80–100 m and *Echinosquilla guerini* is found to 200 m (Ahyong, 2001). Some of the deepest small gonodactylids seem to have changed their predatory behavior and concentrate on small prey taken in the water column or prey that does not require heavy smashing (R.L.C., personal observation). There are, of course, multiple

explanations for these depth distribution patterns. For example, mineralization is more difficult in colder deep water, such that mollusks and crustaceans are not as well-mineralized (Vermeij, 1987) and powerful hammers may be neither necessary nor possible.

The inherent challenges in the design of a failure-resistant, biological hammer may explain why, outside of stomatopods, relatively few species hammer shells (Currey, 1967; Vermeij, 1987). It is intriguing that mantis shrimp do not fracture their own exoskeleton during these strikes. Mantis shrimp raptorial appendages show wear over time and they molt regularly to grow a new exoskeleton. Nonetheless, in between molts, smasher mantis shrimp generate tens of thousands of blows (Caldwell et al., 1989; Full et al., 1989) with a destructive combination of high impacts and implosive cavitation events. In addition to shell hammering, many stomatopods also strike rocks, coral and coralline algae for den construction. This raises fundamental questions as to the mechanical and material properties of the dactyl heel, about which we know little.

Currey et al. (1982) examined the raptorial appendages of an alcohol-preserved *Gonodactylus* specimen and found that the outer layer of the dactyl heel is highly calcified and covers a layer of fibrous cuticle, within which soft tissue is located. Microhardness tests yielded higher values along the outermost cuticular layer, as compared to the inner fibrous layer. Interestingly, microhardness correlated positively with the ratio of phosphorus to calcium in the heel's surface. Currey et al. (1982) also noted that the outermost layer was highly brittle, but that cracks did not propagate into the fibrous layer. Further studies of material and mechanical properties of the mantis shrimp's limb may hold clues for engineered materials that are resistant to both cavitation and impact forces.

It is not presently known how and whether shells respond differently to crushing forces, impact forces and cavitation forces. Mantis shrimp evolved a ballistic raptorial appendage during the Carboniferous (Schöllmann, 2004, F. Schram, personal communication), and a true smashing appendage at least by the Eocene, in what appears to be an odotondactylid (C. Hof, personal communication). It is possible that this unusual method of breaking snails has played an important, but currently unexamined, role in the evolution of shell form in stomatopod prey populations. Mantis shrimp provide a remarkable example of biological cavitation coupled with high impact forces which, in combination, appear to be tremendously effective in fracturing shells.

We are grateful to the following people for suggestions, comments and assistance: J. Baio, J. Birch, N. Danos, M. Dickinson, R. Dudley, R. Full, D. Goldman, W. Korff, M. McHenry, S. Revzen, B. Swanson, J. Tseng, N. Valencia, W. Van Trump, Caldwell Lab., Dickinson Lab., Full Lab., M. Wake Lab., I. B. Biomechanics seminar, and the Miller Institute seminar. We also thank two anonymous reviewers for their comments. Funding was provided by the Miller Institute for Basic Research in Science.

References

Ahyong, S. T. (2001). *Revision of the Australia Stomatopod Crustacea*. Sydney: Australian Museum.

Alexander, R. M. (1985). The maximum forces exerted by animals. *J. Exp. Biol.* **115**, 231-238.

Beal, B. F. (1983). Predation of juveniles by the hard clam *Mercenaria mercenaria* (Linne) by the snapping shrimp *Alpheus heterochaelis* Say and *Alpheus normanni* Kingsley. *J. Shellfish Res.* **3**, 1-9.

Brennen, C. E. (1995). *Cavitation and Bubble Dynamics*. New York: Oxford University Press.

Burrows, M. (1969). The mechanics and neural control of the prey capture strike in the mantid shrimps *Squilla* and *Hemisquilla*. *Z. Vergl. Physiol.* **62**, 361-381.

Burrows, M. and Hoyle, G. (1972). Neuromuscular physiology of the strike mechanism of the mantis shrimp, *Hemisquilla*. *J. Exp. Zool.* **179**, 379-394.

Butler, R. W. and Kirbyson, J. W. (1979). Oyster predation by the black oystercatcher in British Columbia. *Condor* **81**, 433-435.

Caldwell, G. E., Robertson, D. G. E. and Whittlesey, S. N. (2004). Forces and their measurement. In *Research Methods in Biomechanics* (ed. D. G. E. Robertson). Champaign, IL: Human Kinetics.

Caldwell, R. L. (1975). Ecology and evolution of agonistic behavior in stomatopods. *Naturwissenschaften* **62**, 214-222.

Caldwell, R. L., Roderick, G. K. and Shuster, S. M. (1989). Studies of predation by *Gonodactylus bredini*. In *Biology of Stomatopods*, Vol. 3 (ed. E. A. Ferrero), pp. 117-131. Modena: Mucchi.

Ceccio, S. L. and Brennen, C. E. (1991). Observations of the dynamics and acoustics of travelling bubble cavitation. *J. Fluid Mech.* **233**, 633-660.

Coombs, W. P., Jr (1979). Osteology and myology of the hindlimb in the Ankylosauria (Reptilia, Ornithischia). *J. Paleontol.* **53**, 666-684.

Currey, J. D. (1967). The failure of exoskeletons and endoskeletons. *J. Morphol.* **123**, 1-16.

Currey, J. D., Nash, A. and Bonfield, W. (1982). Calcified cuticle in the stomatopod smashing limb. *J. Mater. Sci.* **17**, 1939-1944.

Full, R. J., Caldwell, R. L. and Chow, S. W. (1989). Smashing energetics: prey selection and feeding efficiency of the stomatopod, *Gonodactylus bredini*. *Ethology* **81**, 134-147.

Grubich, J. R. (2000). Crushing motor patterns in drum (Teleostei: Sciaenidae): functional novelties associated with molluscivory. *J. Exp. Biol.* **203**, 3161-3176.

Harvey, P. D. (1985). *Engineering Properties Of Steel.* Metals Park, Ohio: American Society for Metals.

Herrel, A., O'Reilly, J. C. and Richmond, A. M. (2002). Evolution of bite performance in turtles. *J. Evol. Biol.* **15**, 1083-1094.

Ikeda, T. and Ohtsu, M. (1992). Detection of xylem cavitation in field-grown pine trees using the acoustic-emission technique. *Ecol. Res.* **7**, 391-395.

Kaiser, M. J., Hughes, R. N. and Reid, D. G. (1990). Chelal morphometry, prey-size selection and aggressive competition in green and red forms of *Carcinus maenas* (L.). *J. Exp. Mar. Biol. Ecol.* **140**, 121-134.

Korff, W. L. and Wainwright, P. C. (2004). Motor pattern control for increasing crushing force in the striped burrfish (*Chilomycterus schoepfi*). *Zoology* **107**, 335-346.

Lohse, D., Schmitz, B. and Versluis, M. (2001). Snapping shrimp make flashing bubbles. *Nature* **413**, 477-478.

Lush, P. A. and Angell, B. (1984). Correlation of cavitation erosion and sound pressure level. *J. Fluid. Eng.* **106**, 347-351.

Manning, R. B. (1967). Review of the genus *Odontodactylus* (Crustacea: Stomatopoda). *Proc. US Natn. Mus.* **123**, 1-35.

Martin, C. S., Medlarz, H., Wiggert, D. C. and Brennen, C. (1981). Cavitation inception in spool valves. *Trans. ASME* **103**, 564-576.

McNeill, P., Burrows, M. and Hoyle, G. (1972). Fine structures of muscles controlling the strike of the mantis shrimp, *Hemisquilla*. *J. Exp. Zool.* **179**, 395-416.

Meyers, M. A. (1994). *Dynamic Behavior of Materials*. New York: John Wiley and Sons.

Milburn, J. A. (1970). Cavitation and osmotic potentials of *Sordaria* ascospores. *New Phytol.* **69**, 133-141.

Money, N. P., Caesar-TonThat, T.-C., Frederick, B. and Henson, J. M. (1998). Melanin synthesis is associated with changes in hyphopodial turgor, permeability, and wall rigidity in *Gaeumannomyces graminis* var. *graminis*. *Fungal Genet. Biol.* **24**, 240-251.

Moody, K. E. and Steneck, R. S. (1993). Mechanisms of predation among large decapod crustaceans of the Gulf of Maine coast: functional vs. phylogenetic patterns. *J. Exp. Mar. Biol. Ecol.* **168**, 111-124.

Ozkaya, N. and Nordin, M. (1999). *Fundamentals of Biomechanics: Equilibrium, Motion and Deformation*. New York: Springer.
Patek, S. N., Korff, W. L. and Caldwell, R. L. (2004). Deadly strike mechanism of a mantis shrimp. *Nature* **428**, 819-820.
Perks, M. P., Irvine, J. and Grace, J. (2004). Xylem acoustic signals from mature *Pinus sylvestris* during an extended drought. *Ann. For. Sci.* **61**, 1-8.
Preston, S. J., Revie, I. C., Orr, J. F. and Roberts, D. (1996). A comparison of the strengths of gastropod shells with forces generated by potential crab predators. *J. Zool.* **238**, 181-193.
Retamal, M. A. (2002). *Odontodactylus hawaiiensis* Manning, 1967 (Stomatopoda, Gonodactylidae) in Chilean waters. *Gayana* **66**, 73-75.
Ritman, K. T. and Milburn, J. A. (1990). The acoustic detection of cavitation in fern sporangia. *J. Exp. Bot.* **41**, 1157-1160.
Schöllmann, L. (2004). Archaeostomatopodea (Malacostraca, Hoplocarida) from the Namurian B (Upper Marsdenian, Carboniferous) of Hagen-Vorhalle (NRW, Germany) and a redescription of some species of the family Tyrannophontidae. *Geologie und Paläontologie in Westfalen* **62**, 111-141.
Shima, A., Takayama, K. and Tomita, Y. (1983). Mechanism of impact pressure generation from spark-generated bubble collapse near a wall. *AAIA J.* **21**, 55-59.
Smith, A. M. (1991). Negative pressure generated by octopus suckers: a study of the tensile strength of water in nature. *J. Exp. Biol.* **157**, 257-271.
Smith, A. M. (1994). Xylem transport and the negative pressures sustainable by water. *Ann. Bot.* **74**, 647-651.
Smith, A. M. (1996). Cephalopod sucker design and the physical limits to negative pressure. *J. Exp. Biol.* **199**, 949-958.
Snyder, N. F. R. and Snyder, H. A. (1969). A comparative study of mollusc predation by limpkins, everglade kites, and boat-tailed grackles. *Living Bird* **8**, 177-223.
Taylor, G. M. (2000). Maximum force production: why are crabs so strong? *Proc. R. Soc. Lond. B* **267**, 1475-1480.
Tomita, Y. and Shima, A. (1990). High-speed photographic observations of laser-induced cavitation bubbles in water. *Acustica* **71**, 161-171.
Tomita, Y., Shima, A. and Takahashi, K. (1983). The collapse of a gas bubble attached to a solid wall by a shock wave and the induced impact pressure. *J. Fluid. Eng.* **105**, 341-349.
Tyree, M. T. and Sperry, J. S. (1989). Vulnerability of xylem to cavitation and embolism. *Annu. Rev. Plant Physiol. Plant Mol. Biol.* **40**, 19-38.
Tyree, M. T., Dixon, M. A., Tyree, E. L. and Johnson, R. (1984). Ultrasonic acoustic emissions from the sapwood of cedar and hemlock. *Plant Physiol.* **75**, 988-992.
Unsworth, A., Dowson, D. and Wright, V. (1971). 'Cracking joints': A bioengineering study of cavitation in the metacarpophalangeal joint. *Ann. Rheum. Dis.* **30**, 348-358.
Vermeij, G. J. (1987). *Evolution and Escalation: An Ecological History of Life*. Princeton: Princeton University Press.
Vermeij, G. J. and Currey, J. D. (1980). Geographical variation in the strength of thaidid snail shells. *Biol. Bull.* **158**, 383-389.
Versluis, M., Schmitz, B., von der Heydt, A. and Lohse, D. (2000). How snapping shrimp snap: through cavitating bubbles. *Science* **289**, 2114-2117.
Vincent, J. (1990). *Structural Biomaterials.* Princeton: Princeton University Press.
Voight, J. R. (2000). A deep-sea octupus (*Graneledone* cf. *boreopacifica*) as a shell-crushing hydrothermal vent predator. *J. Zool.* **252**, 335-341.
Walker, J. D. (1975). Karate strikes. *Am. J. Phys.* **43**, 845-849.
Wilk, S. R., McNair, R. E. and Feld, M. S. (1983). The physics of karate. *Am. J. Phys.* **51**, 783-790.
Young, F. R. (1999). *Cavitation*. London: Imperial College Press.
Zipser, E. and Vermeij, G. J. (1978). Crushing behavior of tropical and temperate crabs. *J. Exp. Mar. Biol. Ecol.* **31**, 155-172.